ChemComm

RSC Publishing

COMMUNICATION

View Article Online
View Journal | View Issue

Cite this: *Chem. Commun.*, 2013, **49**, 9591

Received 22nd July 2013,
Accepted 20th August 2013

DOI: 10.1039/c3cc45536j

www.rsc.org/chemcomm

Super-hydrophobic yolk–shell nanostructure with enhanced catalytic performance in the reduction of hydrophobic nitroaromatic compounds†

Song Shi,[ab] Min Wang,[a] Chen Chen,[a] Jin Gao,[a] Hong Ma,[a] Jiping Ma[a] and Jie Xu*[a]

A self-templating method to fabricate a super-hydrophobic yolk–shell nano-reactor was reported. Metal nanoparticles were encapsulated in the porous super-hydrophobic shell. This super-hydrophobic catalyst showed excellent performance in the reduction of nitroaromatic compounds in aqueous phase and a positive correlation was found between the reaction rate and the hydrophobicity of the substrate.

Yolk–shell or rattle-type nanoparticles containing a void space between the core and the outer shell have attracted widespread attention due to their tunable optical, electrical and magnetic properties, and hence have wide potential applications in biomedicine, lithium-ion batteries, sensors and nano-reactors.[1–4] In the case of nano-reactors, the shell is of importance for catalysis in virtue of protecting the core nanoparticle from growing, controlling mass transfer or functionalization with active sites.[5–7] Moreover, with the core and the shell having different catalytic active species, the cascade reaction can be achieved using the yolk–shell nano-reactor.[8] To date, a lot of strategies have been developed to fabricate yolk–shell catalysts focusing on the control of composition, pore structures and functionality of the shells to accommodate specific applications.[9–18] Mesoporous yolk–shell nanoparticles were produced by Shi *et al. via* a so-called "structural difference-based" selective etching strategy. Zheng and co-workers found that the etching of the solid silica core can be accelerated by cationic surfactants so as to form the structure.[19] Yin *et al.* developed the surface protection strategy to form the hollow or yolk–shell structure with PVP.[20] Through the post water etching, mono-dispersed yolk–shell nanoparticles were obtained by Mou *et al.*[21] However, to the best of our knowledge, all these methods lead to hydrophilic shells. The control of the hydrophobic properties of the shell to tune the catalytic performance was rarely studied.

The control of material surface hydrophobicity, especially for super-hydrophobic surfaces with a water contact angle (WCA) larger than 150°, is very important and has recently aroused wide research interest.[22,23] Particularly in catalysis, the surface hydrophilic–hydrophobic properties of catalysts played an important role in heterogeneous catalytic reaction.[24–26] Recently, our group has carried out research on the hydrophobic effect in the oxidation process.[27,28] For the yolk–shell nano-reactor, the shell directly controls the mass transfer of the substrate towards the active center. Thus, the control of hydrophilicity–hydrophobicity of the shell is vital for the performance of catalysts.

Very recently, we described the preparation of organic groups containing hollow silica nanospheres *via* a self-templating method. Herein, based on the previous work, a facile strategy to prepare a yolk–shell nano-reactor with a super-hydrophobic shell was reported. With the introduction of the organic groups, the shell shows super-hydrophobicity with WCA of up to 158°. This super-hydrophobic nano-reactor shows a higher reaction rate in the reduction of hydrophobic nitroaromatic compounds in aqueous phase.

The synthesis of the super-hydrophobic yolk–shell nanoparticle employed the self-templating method with the help of isobutyl groups (Scheme 1). Firstly, the Au nanoparticles (Au NPs) with the average diameter of about 13 nm were synthesized according to the previous report (Fig. S1, ESI† and Fig. 1a).[10] The UV-vis absorption peak of Au appears at 528 nm (Fig. S6, ESI†), which is assigned to a plasmon resonance band of spherical gold nanoparticles.[29] Then, Au NPs were covered with silica shells with tetraethyl orthosilicate (TEOS) and isobutyltrimethoxysilane (IBMS) using the Stöber method to form the core–shell structure (Au@IB–SiO_2). One gold core was observed at the centre of the sphere (Fig. 1b) and the diameter of mono-dispersed

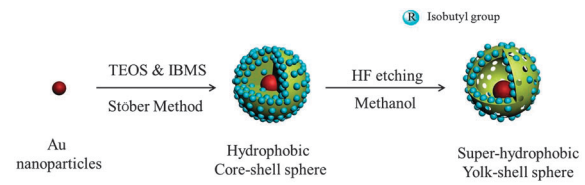

Scheme 1 Procedures for preparation of Au@IB–YSN.

[a] *Dalian National Laboratory for Clean Energy, State Key Laboratory of Catalysis, Dalian Institute of Chemical Physics, Chinese Academy of Sciences, Dalian, 116023, P. R. China. E-mail: xujie@dicp.ac.cn; Fax: +86-411-84379245; Tel: +86-411-84379245*

[b] *Graduate University of Chinese Academy of Sciences, Beijing, 100049, P. R. China*

† Electronic supplementary information (ESI) available: Experimental details, FT-IR, UV-vis, XRD, N_2 adsorption isotherms and size distribution of the particles. See DOI: 10.1039/c3cc45536j

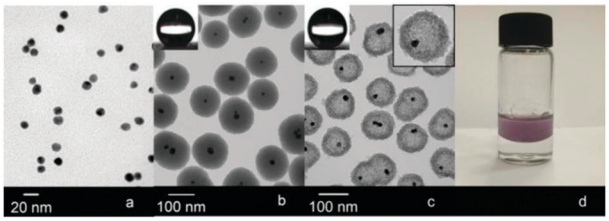

Fig. 1 TEM images of (a) Au NPs, (b) Au@IB–SiO_2, (c) Au@IB–YSN, and (d) Au@IB–YSN distribution between water and cyclohexane.

Au@IB–SiO_2 was about 140 nm (Fig. S2, ESI†). The isobutyl groups were successfully immobilized in the shell as characterized by Fourier transform infrared spectroscopy (FT-IR) and ^{29}Si magic-angle spinning nuclear magnetic resonance (^{29}Si MAS NMR) (Fig. S9a, ESI† and Fig. 2a). In FT-IR spectrum, the appearance of C–H band vibration peaks at 2870 and 2960 cm^{-1} indicated the introduction of isobutyl groups. And in the ^{29}Si MAS NMR spectrum, the peaks at about −100 and −110 ppm were assigned to $HOSi(OSi)_3$ (Q^3 signal) and $(OSi)_4$ (Q^4 signal) species, respectively. In addition, the appearance of organosilane signals at about −65 ppm (T^3 = $IBSi(OSi)_3$) is the direct evidence of fully cross-linked organosiloxane species in agreement with the FT-IR results, which is crucial for surface hydrophobicity.[27,30] The introduction of organic groups made Au@IB–SiO_2 show hydrophobicity with a WCA of 143° (Fig. 1b). Due to coating of the silica shells, the plasmon resonance band of gold nanoparticles in Au@IB–SiO_2 shifted from 528 to 536 nm (Fig. S6, ESI†).[31] The wide-angle X-ray diffraction (XRD) pattern shows five diffraction peaks at 2θ = 38.2°, 44.5°, 64.7°, 77.6° and 81.8° which were assigned to (111), (200), (220), (311) and (222) reflections of the cubic (fcc) gold lattice, respectively, indicating the presence of crystalline gold in the core–shell structure (Fig. S7a, ESI†).[13]

Finally, the obtained core–shell nanoparticle was etched with aqueous HF in methanol to form mono-dispersed Au@IB–YSN yolk–shell nanoparticles (Fig. 1c and Fig. S10, ESI†). The average size of Au@IB–YSN was about 140 nm, which is the same as that of Au@IB–SiO_2 (Fig. S4, ESI†). This phenomenon suggested that the etching process was performed mainly from the inner part. And according to our previous report, this phenomenon was much related to the incorporation of isobutyl groups.[32] Compared with the core–shell nanoparticles, the gold cores in the yolk–shell nanoparticles were not at the centre of the nanoparticles, indicating that the core is movable in the nanoparticle. No growth of gold nanoparticles was observed in the etching process and the average size was also 13 nm (Fig. S5, ESI†). The state of Au nanoparticles in Au@IB–YSN was also characterized by XRD and is found to be the same as that of Au@IB–SiO_2 (Fig. S7b, ESI†). The peak in UV-vis spectrum at 530 nm confirmed little change in Au nanoparticles (Fig. S6c, ESI†). Compared with Au@IB–SiO_2, the Au content increased from 2.1% to 8.6% in Au@IB–YSN due to the partly etching of the shell. The characteristic peak of C–H band vibration absorption (2870 and 2960 cm^{-1}) still existed (Fig. S9b, ESI†), illustrating that the isobutyl groups remained after etching. Compared with the FT-IR spectrum of Au@IB–SiO_2, the peak at 950 cm^{-1} decreased for Au@IB–YSN, suggesting the decrease in Si–OH content. These results were further confirmed by ^{29}Si MAS NMR (Fig. 2b). The T^3 signal illustrated that the isobutyl groups were still present. In addition, the Q^3 signal was much weaker for Au@IB–YSN than that of Au@IB–SiO_2, confirming the decrease in Si–OH content. The decrease in Si–OH content increased the hydrophobicity of Au@IB–YSN with WCA of up to 158°. In a water–cyclohexane mixed solvent, Au@IB–YSN selectively distributed in the upper cyclohexane phase, indicating the hydrophobic nature of Au@IB–YSN (Fig. 1d).

The porous property of Au@IB–YSN was measured by N_2 adsorption–desorption measurement (Fig. S8, ESI†). Au@IB–YSN showed a high specific surface area of 547 $m^2\ g^{-1}$. The isotherm of Au@IB–YSN shows type IV loops suggesting mesoporous structure of Au@IB–YSN (Fig. S8, ESI†). From N_2 adsorption–desorption measurement, the average pore-size of Au@IB–YSN is found to be about 5 nm. These mesopores should be produced during the etching process, which accounted for the wide pore size distribution as shown in Fig. S8 (ESI†). This phenomenon corresponded with the etching method used in the other report.[33] The mesoporous shell made the molecules easily penetrate the shell and reach the Au core, which pave the way for application in catalysis.

This method is versatile and could synthesize a wide range of yolk–shell structures with different metal cores and sizes. For example, Pt nanoparticles can also be incorporated into the super-hydrophobic shell using a similar method (Fig. S15, ESI†). In addition, the metal size could also be adjusted. Yolk–shell nanoreactors with 6 nm and 40 nm Au nanoparticles were also prepared (Fig. S11–S14, ESI†). Therefore, the above-mentioned method provides possible access to a wide range of super-hydrophobic yolk–shell nano-reactors and is intriguing for catalysis.

As for the heterogeneous catalysis process, the mass transfer directly influences the catalytic performances. The reactant must diffuse into the support and reach the active site where catalytic reaction occurs.[13,34] Since Au@IB–YSN has excellent water repellent and oilphilic properties, it could be used to enrich organic compounds in aqueous phase to accelerate the reaction rate. The catalytic performance of Au@IB–YSN in the reduction of 4-nitrophenol (4-NP) by $NaBH_4$ in aqueous phase was investigated as a model reaction (Fig. 3a).[9] As reported elsewhere, $NaBH_4$ does not reduce 4-NP in the absence of the Au catalyst. Since the concentration of $NaBH_4$ was much higher than that of 4-NP, the reaction can be considered as a pseudo-first-order reaction. It was found that the relationship between $\ln(C_t/C_0)$ and reaction time fits pseudo-first-order kinetics. The apparent rate constant K_{app} was $7.7 \times 10^{-3}\ s^{-1}$ (Fig. S19, ESI†). Another two control catalysts prepared using the wet impregnation method with the same Au diameter were also tested

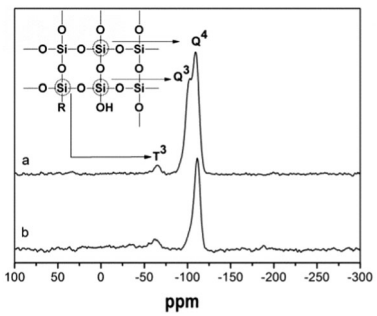

Fig. 2 ^{29}Si MAS NMR of (a) Au@IB–SiO_2 and (b) Au@IB–YSN.

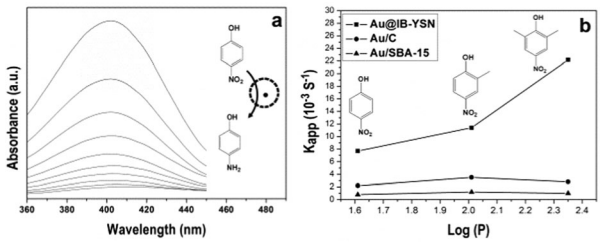

Fig. 3 (a) Time-dependent UV-vis spectra of 4-NP reduction in the presence of Au@IB–YSN and (b) catalytic activity towards the substrate with different hydrophobicity of Au@IB–YSN, Au/C and Au/SBA-15.

for this reaction (Fig. S16 and S17, ESI†). Though they were also porous materials with high BET surface areas, their catalytic reaction rate was much lower than that of the mono-dispersed super-hydrophobic Au@IB–YSN due to their hydrophilic characteristics. The K_{app} values were only 1.0×10^{-3} s^{-1} and 2.2×10^{-3} s^{-1} for Au/SBA-15 and Au/C, respectively (Fig. S22 and S25, ESI†). To further confirm the hydrophobic effect on the reaction rate in aqueous phase, 2-methyl-4-nitrophenol (2-M-4-NP) and 2,6-dimethyl-4-nitrophenol (2,6-2M-4NP) with higher hydrophobicity were selected to perform the reduction (hydrophobicity is reflected by log *P*).[35] As shown in Fig. 3b, hydrophilic Au/C and Au/SBA-15 show a similar reaction rate for the three nitroaromatic compounds. In contrast, in the case of super-hydrophobic Au@IB–YSN, the reaction rate was positively correlated with log *P* of the substrate. The reaction rate of 2-M-4-NP and 2,6-2M-4NP reached 11.4×10^{-3} s^{-1} and 22.2×10^{-3} s^{-1}, respectively (Fig. S20 and S21, ESI†). The more hydrophobic the substrate is, the higher reaction rate it achieved. The size effect of gold NPs can be neglected since the sizes of Au NPs were the same (Fig. S16 and S17, ESI†). Our results suggest that the difference in reaction rates is attributed to the hydrophobic and oilphilic properties of the support as illustrated by WCA and the dispersed experiment. As seen in Fig. 1d and Fig. S18 (ESI†), the obtained super-hydrophobic yolk–shell nanoparticles well dispersed in cyclohexane phase, which means they are oilphilic, while Au/C and Au/SBA-15 dispersed in water phase, confirming their hydrophilicity. In the aqueous reaction, the oilphilic shell shows high affinity towards organic compounds than towards the water molecule. Therefore, the organic compound will be enriched in Au@IB–YSN nanoparticles, thus enhancing the reaction rate. The more hydrophobic the compound is, the larger is the adsorption rate difference between the organic compound and the water molecule.[36] This finally resulted in a higher reaction rate as seen in Fig. 3b. In contrast, for the hydrophilic catalyst, the water molecule will be easily adsorbed on the surface which will hinder the adsorption of the organic compound and lead to a low reaction rate. These phenomena showed that the super-hydrophobic yolk–shell catalysts had the advantage over the hydrophilic catalyst in the aqueous reaction of organic compounds. In addition, the catalyst could be reused at least 2 times, and the yolk–shell structure was still retained and the Au NPs did not grow larger obviously (Fig. S28 and S29, ESI†).

In conclusion, a simple self-templating method was developed to prepare super-hydrophobic nano-reactors. The type and the size of the core can be easily adjusted. The super-hydrophobic yolk–shell catalyst with Au NPs shows high affinity towards organic substrates in aqueous phase and shows high reaction rate towards the reduction of nitroaromatic compounds in aqueous phase. And a positive correlation was found between the reaction rate and the hydrophobicity of the substrate.

This work was supported by the National Natural Science Foundation of China (Grant no. 21103175, 21103206 and 21233008).

Notes and references

1 J. Liu, S. Z. Qiao, J. S. Chen, X. W. Lou, X. Xing and G. Q. Lu, *Chem. Commun.*, 2011, **47**, 12578–12591.
2 F. Q. Tang, L. L. Li and D. Chen, *Adv. Mater.*, 2012, **24**, 1504–1534.
3 X. Li, Y. Yang and Q. Yang, *J. Mater. Chem. A*, 2013, **1**, 1525.
4 J. Liu, Y. Zhou, J. Wang, Y. Pan and D. Xue, *Chem. Commun.*, 2011, **47**, 10380–10382.
5 S.-H. Wu, C.-T. Tseng, Y.-S. Lin, C.-H. Lin, Y. Hung and C.-Y. Mou, *J. Mater. Chem.*, 2011, **21**, 789.
6 Z. Chen, Z.-M. Cui, P. Li, C.-Y. Cao, Y.-L. Hong, Z.-y. Wu and W.-G. Song, *J. Phys. Chem. C*, 2012, **116**, 14986–14991.
7 P. M. Arnal, M. Comotti and F. Schuth, *Angew. Chem., Int. Ed.*, 2006, **45**, 8224–8227.
8 Y. Yang, X. Liu, X. Li, J. Zhao, S. Bai, J. Liu and Q. Yang, *Angew. Chem., Int. Ed.*, 2012, **51**, 9164–9168.
9 Y. Deng, Y. Cai, Z. Sun, J. Liu, C. Liu, J. Wei, W. Li, C. Liu, Y. Wang and D. Zhao, *J. Am. Chem. Soc.*, 2010, **132**, 8466–8473.
10 M. Wang, J. Ma, C. Chen, F. Lu, Z. Du, J. Cai and J. Xu, *Chem. Commun.*, 2012, **48**, 10404–10406.
11 J. Qi, J. Chen, G. Li, S. Li, Y. Gao and Z. Tang, *Energy Environ. Sci.*, 2012, **5**, 8937.
12 J. Liu, H. Q. Yang, F. Kleitz, Z. G. Chen, T. Yang, E. Strounina, G. Q. M. Lu and S. Z. Qiao, *Adv. Funct. Mater.*, 2012, **22**, 591–599.
13 J. Guo and K. S. Suslick, *Chem. Commun.*, 2012, **48**, 11094–11096.
14 Y. Yang, J. Liu, X. Li, X. Liu and Q. Yang, *Chem. Mater.*, 2011, **23**, 3676–3684.
15 J. Lee, J. C. Park and H. Song, *Adv. Mater.*, 2008, **20**, 1523–1528.
16 X.-J. Wu and D. Xu, *Adv. Mater.*, 2010, **22**, 1516–1520.
17 T. Yang, J. Liu, Y. Zheng, M. J. Monteiro and S. Z. Qiao, *Chem.–Eur. J.*, 2013, **19**, 6942–6945.
18 J. Liu, S. Z. Qiao, S. Budi Hartono and G. Q. Lu, *Angew. Chem., Int. Ed.*, 2010, **49**, 4981–4985.
19 X. L. Fang, Z. H. Liu, M. F. Hsieh, M. Chen, P. X. Liu, C. Chen and N. F. Zheng, *ACS Nano*, 2012, **6**, 4434–4444.
20 Q. Zhang, J. P. Ge, J. Goebl, Y. X. Hu, Z. D. Lu and Y. D. Yin, *Nano Res.*, 2009, **2**, 583–591.
21 Y. S. Lin, S. H. Wu, C. T. Tseng, Y. Hung, C. Chang and C. Y. Mou, *Chem. Commun.*, 2009, 3542–3544.
22 K. S. Liu and L. Jiang, *Nanoscale*, 2011, **3**, 825–838.
23 T. L. Sun, L. Feng, X. F. Gao and L. Jiang, *Acc. Chem. Res.*, 2005, **38**, 644–652.
24 C. Chen, J. Xu, Q. Zhang, Y. Ma, L. Zhou and M. Wang, *Chem. Commun.*, 2011, **47**, 1336–1338.
25 K. Inumaru, M. Murashima, T. Kasahara and S. Yamanaka, *Appl. Catal., B*, 2004, **52**, 275–280.
26 A. Corma, M. Domine, J. A. Gaona, J. L. Jorda, M. T. Navarro, F. Rey, J. Perez-Pariente, J. Tsuji, B. McCulloch and L. T. Nemeth, *Chem. Commun.*, 1998, 2211–2212.
27 M. Wang, C. Chen, J. P. Ma and J. Xu, *J. Mater. Chem.*, 2011, **21**, 6962–6967.
28 C. Chen, J. Xu, Q. H. Zhang, H. Ma, H. Miao and L. P. Zhou, *J. Phys. Chem. C*, 2009, **113**, 2855–2860.
29 L. Tan, D. Chen, H. Liu and F. Tang, *Adv. Mater.*, 2010, **22**, 4885–4889.
30 D. J. Yang, Y. Xu, D. Wu, Y. H. Sun, H. Y. Zhu and F. Deng, *J. Phys. Chem. C*, 2007, **111**, 999–1004.
31 Y. Chen, H. Chen, L. Guo, Q. He, F. Chen, J. Zhou, J. Feng and J. Shi, *ACS Nano*, 2010, **4**, 529–539.
32 S. Shi, M. Wang, C. Chen, F. Lu, X. Zheng, J. Gao and J. Xu, *RSC Adv.*, 2013, **3**, 1158–1164.
33 Y. Chen, Y. Gao, H. R. Chen, D. P. Zeng, Y. P. Li, Y. Y. Zheng, F. Q. Li, X. F. Ji, X. Wang, F. Chen, Q. J. He, L. L. Zhang and J. L. Shi, *Adv. Funct. Mater.*, 2012, **22**, 1586–1597.
34 J. Lee, J. C. Park, J. U. Bang and H. Song, *Chem. Mater.*, 2008, **20**, 5839–5844.
35 Log *P* is the log of the Hansch coefficient of hydrophobicity, *i.e.*, the octanol/water partition coefficient and it is usually used to reflect the hydrophobicity of the compound. A. Leo, C. Hansch and D. Elkins, *Chem. Rev.*, 1971, **71**, 525–616.
36 C. Zhang, K. Li, S. Song and D. Xue, *Chem.–Eur. J.*, 2013, **19**, 6329–6333.